Atom vacancy lines and surface patterning: The role of stress for Br-Si(100)-(2×1) at 700 K

G. J. Xu, E. Graugnard,* B. R. Trenhaile, Koji S. Nakayama, and J. H. Weaver
Department of Materials Science and Engineering, Department of Physics, and Frederick Seitz Materials Research Laboratory, University of Illinois at Urbana-Champaign, Urbana, Illinois 61801, USA
(Received 27 March 2003; published 1 August 2003)

Using variable-temperature scanning tunneling microscopy, we studied Br-induced roughening of Si(100)-(2 ×1) at 700 K. The roughening pathway requires Br-free dimers so that a saturated surface is inactive. Initial roughening involves the formation of atom vacancy lines and regrowth chains of Si dimers on the terraces. The atom vacancy lines grow longer through a stress-induced process that creates dimer vacancies. Br adatom repulsion then splits these dimer vacancies into pairs of single-atom vacancies. A (3×2) reconstruction derived from dimer rows and atom vacancy lines is energetically favored at high concentration due to Br-Br repulsive interactions and Br bond angle relaxation that is facilitated by the (3×2) structure. Though favored, the conversion is slow at high coverage. Continuous scanning over ∼72 h shows the correlation between Br concentration and surface morphology. Ultimately, a highly dynamic configuration is reached in which large regrowth islands and large terrace areas have (3×2) symmetry. These areas become unstable when the Br concentration drops below a critical value and conversion to (2×1) terraces and extended islands occurs.

DOI: 10.1103/PhysRevB.68.075301 PACS number(s): 68.37.Ef, 68.35.Ja, 81.65.Cf

I. INTRODUCTION

With the focus on nanoscale science and technology, new techniques have been developed to pattern and fabricate features at smaller length scales. Self-assembly processes have received much attention because they offer the possibility that device structures can build themselves.[1] Most studies of *in vacuo* self-assembly have focused on material deposition where growth is directed and stabilized at the atomic level, including the formation of atom wires at steps,[2,3] quantum dots,[4,5] rare-earth silicide wires,[6,7] and Bi nanowires.[8,9] Far less attention has been paid to atomic-scale patterning associated with material removal (etching) though directed growth of the vacancy structures also plays an important role.[10] Here, we explore halogen-induced patterning of Si(100)-(2×1) where we find directed growth of pairs of atom vacancy lines (AVL's) under conditions where the surface is nearly saturated with Br. These novel features have remarkable aspect ratios, exceeding 300, and their formation has implications on later stages of surface evolution including (3×2) patterning and surface roughening.

Scanning tunneling microscopy (STM) has been used extensively to reveal the morphologies that result from halogen reactions with silicon surfaces, generally using samples etched at high temperature and imaged at room temperature.[11–14] Based on studies with Cl and Br on Si(100), models have been developed that relate the atomic-level sequence of events involved in reactions and dihalide desorption to the surface morphologies.[15–20] While similarities have been demonstrated for Cl- and Br-Si(100), important differences have also been discovered. For example, the morphologies and etch rates at high coverage are very different because the Br system can follow a reaction pathway at 800 K that is inaccessible to Cl.[18]

Recently, we reported a surprising roughening phenomenon for Cl-Si(100) that was not accompanied by dichloride desorption, i.e., surface roughening without etching.[20] This roughening occurred at a temperature well below that needed to activate desorption, where the system was assumed to be static. Such enhanced dynamics force a rethinking of surface reactions, the role of reactive adsorbates, and their stability in general. Here, we focus on the Br-Si system at 700 K to gain further insight into roughening and competing pathways and to determine differences related to the strength of the halogen-halogen repulsive interaction. With STM, we follow the directed growth of atom vacancy lines, (3×2) patterning, regrowth chain formation, and then the more dynamic changes that accompany gradual depletion of Br. Br-Br repulsive interactions constitute the main driving force for these changes.[21–23]

Figure 1 depicts two potential energy surfaces that allow some perspective as to what can be expected and how etching differs from roughening or patterning. The pathway in (a) depicts etching for halogens on Si(100). Initially, a dimer with two Br atoms, 2SiBr, undergoes an isomerization reaction to $SiBr_2+Si$, state I. This configuration will generally decay back to 2SiBr. If, however, the Si atom with its two dangling bonds escapes onto the terrace, state II, then the decay pathway for $SiBr_2$ to 2SiBr is eliminated and the probability that the $SiBr_2$ unit will desorb is greatly enhanced. To first order, the energy of the final state is slightly higher than the initial state as one dimer vacancy (DV), one Si adatom on the terrace [Si(a)], and one $SiBr_2$ gas species [$SiBr_2$(g)] are created. The surface can be healed when mobile dimer vacancies and Si adatoms are accommodated at steps. Entropy considerations at elevated temperature drive the system to this final configuration. A necessary condition is that there be halogen-free dimers to accommodate the transferred Si atom. This is the currently accepted model of vacancy-assisted thermal desorption.[14] Dimer vacancies are created, Br is lost as $SiBr_2$(g), and the excess Si(a) on the terrace can form regrowth islands (RI's).

The question to be asked concerning pathway (a) is what will happen if the temperature is too low for desorption. Based on STM studies of Cl-Si(100)-(2×1), we developed pathway (b) which describes a very different final configuration because it envisions surface roughening without desorption. As in (a), steps I and II involve isomerization and es-

 ©2003 The American Physical Society

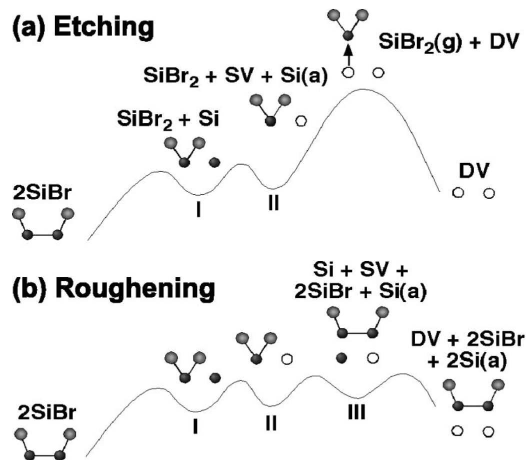

FIG. 1. Potential energy surfaces depicting etching and roughening pathways for halogen-Si(100). In etching (a), a dimer terminated with two Br atoms transforms to state I, $SiBr_2+Si$, and the Si atom escapes onto the terrace, creating state II, $SiBr_2+SV+Si(a)$. This requires a Br-free dimer to accommodate the Si adatom, Si(a). The $SiBr_2$ species can desorb via thermal activation to create a dimer vacancy. Roughening (b) involves the same progression to state II but at a temperature that is too low to activate desorption. In this case, the system can transform to state III by transferring both Br atoms from $SiBr_2$ to bare dimers of the terrace, denoted Si+SV+2SiBr+Si(a). The single Si atom of the original dimer then escapes onto the terrace. The two Br atoms can participate in further reactions. The surface thereby roughens without desorption with DV's and regrowth atoms produced at temperatures where nothing had previously been expected. At low coverage, the DV's and Si(a) species will form large pits and regrowth islands. At high coverage, their diffusion is frustrated.

cape of a Si atom to produce a dihalide unit adjacent to a vacancy but at a temperature that is too low to activate desorption. For Cl-Si(100), we showed that the $SiCl_2$ unit could decay by transferring its two halogen atoms onto halogen-free dimers on the terrace, state III. Once this occurs, the residual Si atom will also transfer to a halogen-free dimmer.[20] Pathway (b) leads to roughening since a dimer vacancy is created, the two Si atoms can form regrowth islands, and the halogen atoms can be used to activate further reactions. The roughening pathway is dominant at low temperature. At higher temperature, there is competition between roughening and etching. In the following, we explore the ramifications of pathway (b) for Br-Si(100)-(2×1).

Using high-temperature imaging, we show that dimer vacancies produced randomly are sufficiently mobile that they can assemble into dimer vacancy lines (DVL's). Once formed, the Br-Br repulsive interactions cause adjacent Si dimers in the dimer vacancy lines to shift by one atomic unit. This creates atom vacancy lines and relaxes the steric repulsions.[24] In turn, elongation is assisted by the high surface stress at the ends of the atom vacancy lines. The atom vacancy line formation mechanism is the same as that for Cl-Si(100),[25] but the atom vacancy lines are more numerous here because the Br-Br steric repulsion is stronger.[26] Thus, stress both lowers the barrier for dimer vacancy creation and is important in atom vacancy line formation.

By following the evolution of the surface over ~72 h, we show the direct connection between the Br concentration and the surface morphology. The results demonstrate an intricate interplay that involves atom vacancy line growth and creation of Si regrowth chains (RC's) on the terrace. After ~9 h at 700 K, elongated regrowth chains coalesce into regrowth islands between regions of atom vacancy lines, with both terraces and islands forming a (3×2) reconstruction. In this configuration, dimer rows are separated by atom vacancy lines, a state favored energetically because of the Br repulsive interactions. As the Br concentration continues to diminish, these (3×2) features begin to transform back to a (2×1) reconstruction. We stress that these dynamic changes occur at a temperature where the etching pathway, Fig. 1(a), is negligible and the surface would have been expected to be passive.

II. EXPERIMENTAL CONSIDERATIONS

The STM experiments were carried out in two separate ultrahigh-vacuum systems (pressures $<5\times10^{-11}$ Torr) containing either a room-temperature STM or a variable temperature STM, both by Omicron NanoTechnology. The samples were p-type Si wafers (B doped, 0.01–0.012 Ω cm, Virginia Semiconductor Inc.) oriented within 0.5° of (100) with a miscut toward [110]. Clean surfaces were prepared using thermal treatments either by electron bombardment or direct current through the sample.[27] Clean surfaces were exposed at room temperature to electrochemical Br cells consisting of a AgBr pellet doped with ~5% $CdBr_2$. The source was operated at a current of 5 μA to emit a beam of 1.6 $\times10^{13}$ molecules/s. The initial and final Br surface concentrations were determined directly from filled-state images acquired at room temperature where bare Si dimers could be readily distinguished from Br-terminated dimers.

Two different experimental protocols were followed. In one, surface modification was activated by heating the exposed samples via electron bombardment while the temperature was monitored by an optical pyrometer. The samples were then cooled to room temperature and transferred to the STM stage for analysis. In the other, the samples were heated on the STM stage at a rate of 10 K/min to 700–750 K. The sample temperature was controlled by a direct current through the sample. The temperature in the STM stage was deduced from the heating power which was calibrated using an optical pyrometer. Images were acquired after the temperature stabilized. When the experiments were completed, the surface was imaged at room temperature to obtain the final Br coverage (Br diffusion made it impossible to quantify the Br coverage at high temperature). All of the images presented here, except Fig. 4(b) and Fig. 5(a), were obtained in the constant-current mode with negative sample bias. The images were acquired with either W or Pt/Ir tips.

III. RESULTS

As the understanding of surface reactions and structural changes has improved for halogens on Si(100), it has become obvious that the halogen concentration is a key param-

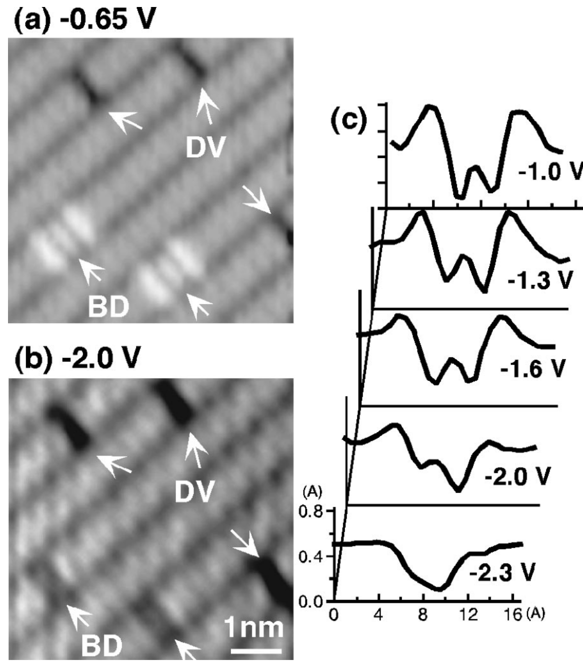

FIG. 2. The bias dependence of nearly saturated Br-Si(100)-(2 $\times 1$) showing three DV's and two bare dimers, BD's. The bare dimer appears as a bright triplet when imaged at -0.65 V; it becomes indistinguishable from a DV at -2.0 V. The DV is dark under both conditions. (c) shows the bias dependence of the height profile of the BD, with a triplet feature well defined at low negative bias.

eter. To be precise in modeling competition between reaction pathways thus requires quantitative information about the concentration. Section III A shows how STM images can be used to directly determine that concentration but also that there are pitfalls which must be avoided. Section III B focuses on the internal structure of atom vacancy lines, showing that the exposed Si atoms dimerize to produce a local (3 $\times 2$) configuration. Section III C discusses the growth dynamics of the atom vacancy lines. Section III D elaborates on surface roughening and its evolution as deduced from images acquired at 700 K over a ~ 72 h period.

A. Determination of surface coverage

Figure 2 shows the bias dependence for nearly saturated Br-Si(100)-(2$\times$1). Figure 2(a) is a filled-state image where dimers with two Br adatoms, 2SiBr, run diagonally (sample bias -0.65 V). The two bare dimers are imaged as three bright features against a background of gray 2SiBr units at -0.65 V. They are dark when imaged with a sample bias of -2.0 V, as in Fig. 2(b). The three dimer vacancies are dark, regardless of bias. This bias dependence is summarized quantitatively in Fig. 2(c) where the three features of the triplet were clear at -1.0 V but they washed out as the bias voltage was changed to -2.3 V. Indeed, the height of the 2SiBr sites adjacent to the central site decreased by 0.3 Å in this voltage range. The triplet feature indicates that the extended π bonding states of the bare Si dimer interact with the Br $4p$ orbitals of Br on adjacent dimers[28] or that the dimers on either side of the bare dimer site relax inward to reduce the repulsive adsorbate-adsorbate interactions from their neighbors. The latter would reduce the gap between the σ bonding and antibonding states of Si-Br, shifting the σ state toward the band edge and resulting in enhanced tunneling (bright feature at low bias voltage). It is the characteristic brightness of the bare dimer triplet that makes it possible to identify bare dimers and to deduce the coverage for Br-Si(100) and Cl-Si(100). Conversely, Fig. 2(b) shows that the triplet is replaced by a dark feature at high bias (-2.0 V) as the tip mainly probes the Br orbitals, and it is difficult to differentiate bare dimers from dimer vacancies.

Figure 3 demonstrates the coverage dependence of the triplet. Analysis of large, high-resolution images indicates that the triplet density increased from 1.8×10^{12} cm^{-2} in Fig. 3(a) to 6.9×10^{13} cm^{-2} in (b) and to 1.0×10^{14} cm^{-2} in (c). For reference, the dimer density of Si(100)-(2$\times$1) is 3.4 $\times 10^{14}$ cm^{-2}. The triplet character for the single bare dimer in (a) is clear as it stands out against ~ 400 2SiBr dimers and 2 DV's. At a coverage of ~ 0.8 monolayer (ML), bare dimers tend to occupy sites diagonally across dimer rows to reduce the steric repulsion between Br-occupied sites. Most of the triplets are isolated though there are also much brighter two- and three-dimer sized features that represent adjacent bare dimer sites, as identified in Fig. 3(b). The change in brightness suggests that the charge distributions are quite different from those of single bare dimers. Bright lines along a dimer row are more common at 0.7 ML. As highlighted in Fig. 3(c), they appear as bright units derived from 3–5 bare dimers. Grouping of bare dimers becomes increasingly common for ~ 0.2 ML where there are many bright lines consisting of bare dimers and some isolated dark 2SiBr features. Comparing with the bright bare lines, when 2SiBr units appear on either side of a single bare dimer, the single bare dimer site is gray, as labeled BD in the lower right in Fig. 3(d). Finally, dimer vacancies tend to quench the dynamic buckling of Br-free dimers, resulting in zigzag rows of asymmetric dimers, as labeled A in Fig. 3(d).

Hermann and Boland[24] recently used STM to obtain surface morphologies of Br-Si(100), imaging with a sample bias of $+1.7$ V (empty states) while concluding that dark features were dimer vacancies. There are two problems with this protocol. The first is a miscounting of dimer vacancy and bare dimer sites, and the second is that Br can be induced to hop on Si(100) by tunneling electrons of energy >0.8 eV. To demonstrate the first, we show images in Fig. 4 that were obtained after a sample like that of Fig. 3(a) was heated to 800 K for 10 min to induce both roughening and etching.[18] The final Br coverage was 0.78 ML. The image in Fig. 4(a) was obtained with a sample bias of -2.5 V (filled states). The bright features are 2SiBr units, the gray features are bare dimers, and the dark features are dimer vacancies. Etching has also produced atom vacancy lines and a dimer vacancy line. The same area was then scanned with sample bias $+2.0$ V (empty states) to obtain Fig. 4(b). Comparison of the features in box I and depicted in Fig. 4(c) shows two gray dimers in (a) that are dark in (b). Thus, bare dimers might be mistaken for dimer vacancies in the images of Ref. 24, and

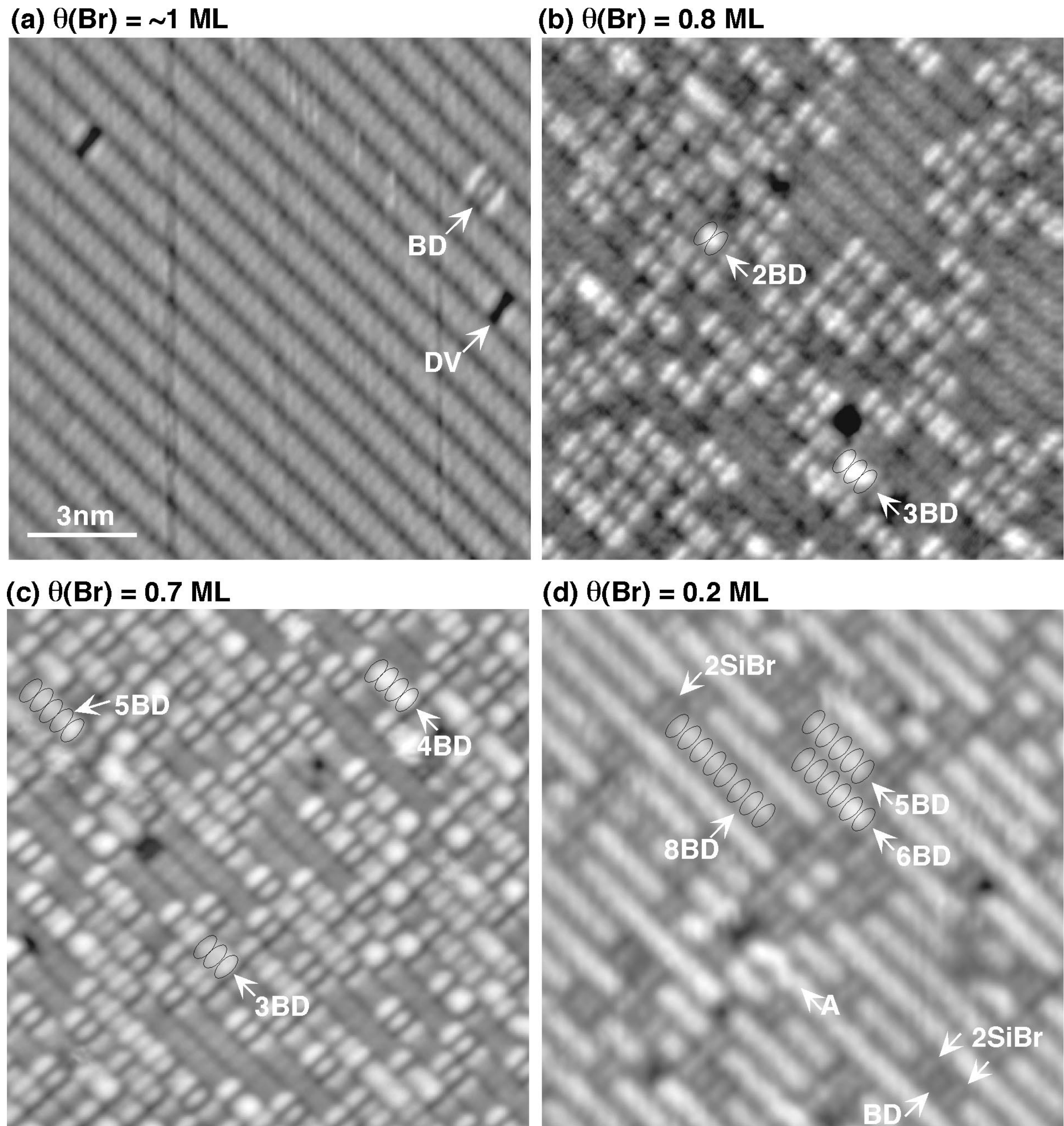

FIG. 3. The coverage dependence of filled-state images for Br-Si(100). In (a), one bare dimer and two DV's are evident against a gray background of 2SiBr rows. Triplets are still evident at 0.8 and 0.7 ML, but BD's also appear as nearest neighbors in rows. At 0.2 ML, the range of possible configurations is greater, as discussed in the text.

high-bias, empty-state images do not provide the needed information regarding coverage.

Box II in Fig. 4 identifies the second problem with positive sample bias imaging. As discussed by Nakayama *et al.*,[28] electrons that tunnel from tip to sample can induce Br hopping if the bias exceeds +0.8 V. The left of Fig. 4(d) shows the configuration of box II in Fig. 4(a) and the right part corresponds to Fig. 4(b). While the structure in the lower row of the image shows no change, multiple movements are apparent for the top row (at least four Br hopping events).

These results demonstrate that the distribution of bare dimers is best obtained from low-voltage negative sample bias results, that care must be exercised in deducing the coverage from high positive sample bias results, and that the chemisorption system is perturbed by positive bias imaging above +0.8 V. For these reasons, the results presented here and in previous papers have favored negative sample bias imaging.

B. Atom vacancy line internal structure: (3×2) vs (3×1)

Atom vacancy lines on Si(100)-(2×1) were first discovered by Chander *et al.* when they investigated etch morphologies as a function of Br fluence at 800–900 K.[11] Pits

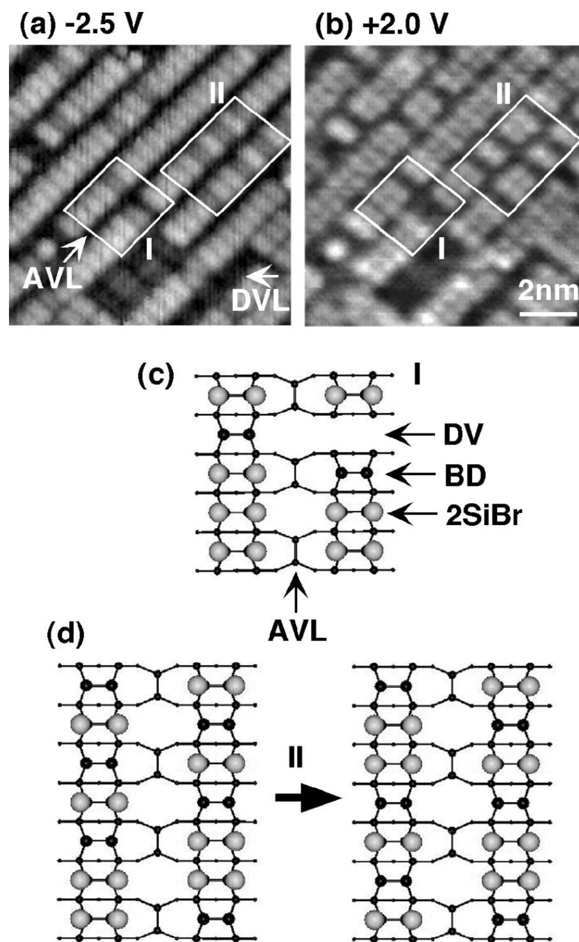

FIG. 4. The sample bias polarity dependence for Br etched Si(100)-(2×1) where there are BD's, dimer vacancy lines (DVL's), atom vacancy lines (AVL's), and pits. The surface was scanned with negative sample bias of -2.5 V (a), and then again with positive sample bias of $+2.0$ V (b). Tunneling current was 0.2 nA. (c) Schematic of box I in (a) and (b). Comparison shows that the two BD's that were gray in (a) were dark in (b). (d) Schematic of the initial and final Br configurations in box II showing that electron injection perturbed the system and caused Br atoms to hop. These results show that coverages can be deduced from negative bias images; the same cannot be said for positive bias results. (Hopping does not affect the coverage, but the way bare dimers appear with positive bias can be misleading.)

and dimer vacancy lines were observed when samples were exposed to low and intermediate doses. Surprisingly, when the dose reached a critical value at 850–900 K, a new structure formed in which parallel lines of atom vacancies were separated by a dimer row and the dimer row was shifted by one atomic unit (3.84 Å) with respect to the rest of the terrace (2×1) dimers. These closely spaced atom vacancy lines appeared in domains with (3×1) local structure. Chander *et al*. concluded that the etch patterns resulted from a high temperature (3×1) adsorption phase on Br-Si(100) where $SiBr_2$ desorption created the missing Si rows. Subsequently, Nakayama *et al*.[18] showed that the (3×1) phase also appeared when Si(100) surfaces with 0.8–1 ML Br were heated to 800 K. They proposed pairwise desorption of $SiBr_2$ with the formation of an intermediate surface structure that can be written as $[SiBr_2\ Si{=}Si\ SiBr_2]$ where dimerization of the two central Si atoms produces Si = Si and prevents decay of $SiBr_2+Si$ into 2SiBr. This increases the likelihood of $SiBr_2$ desorption.

Recently, de Wijs and Selloni[15] challenged the (3×1) classification. They performed first-principles molecular-dynamics calculations based on density functional theory, and they predicted that exposed second layer Si atoms in the atom vacancy lines could dimerize. This would produce a (3×2) reconstruction rather than (3×1), the number of dangling bonds would be reduced, and halogens could adsorb on the remaining dangling bonds in the second layer. Here, we provide evidence of such dimerization. The problem in the past was that the experimental resolution was insufficient to resolve structure in the atom vacancy line.

Figure 5(a) is an empty-state image (+2.0 V sample bias) and Fig. 5(b) is a filled-state image (-1.7 V sample bias) of a surface that was heated to 750 K for 10 min and then imaged at room temperature (initial coverage 0.64 ML).[29] There is a deep minimum between the dimer rows in filled-state images, but it appears along the center of the rows in empty-state images. This shift reflects differences in the bonding and antibonding states probed by the STM tip in the two biases.[30] Two atom vacancy lines have formed, as have several dimer vacancy lines and a small pit. The atom vacancy lines are terminated by a two-dimer-wide pit at each end. The Br adatoms are resolved as individual bright spots in Fig. 5(a). Regions of $c(4\times2)$ symmetry arise when alternate dimers are Br terminated. This structure reflects the repulsive interactions of the adatoms, and it is common for Br and I at intermediate coverage.[18,31,32] A short section of Br-free dimers is outlined by the dashed box at the right of each image, labeled Si, but only filled-state images show that the bare dimers are buckled. This is consistent with the report that the tip mainly probes Si π states under filled-state imaging conditions, but high-bias empty-state imaging reflects mixed electronic states that involve Si π^* and dimer σ^* states.[30] Therefore, intrinsically buckled dimers appear symmetric.

Figure 5(c) shows line profiles along the atom vacancy lines. The profile from (a), the empty-state image, shows clear corrugation with the distance between deep minima, marked with arrows, equal to the spacing between surface dimers (7.7 Å). The profile from (b), the filled-state image, is not as clearly resolved but deep minima separated by ~7.7 Å are still evident. Arrow I shows the center of the dimer rows while arrow II indicates the trough between the dimer rows in the second layer. The deep minima in the empty- and filled-state profiles, arrows I and II, are shifted by ~3.8 Å. Figure 5(d) is a structural schematic of the atom vacancy lines where exposed second layer Si atoms are dimerized.

The two atom vacancy lines in Fig. 5 are nine units in length, and they are terminated by three dimer vacancies at each end. It has been reported that dimer vacancy lines of odd lengths, $2N+1$ dimer vacancies, greatly outnumber those of even lengths, $2N$, because odd lengths offer a rebonded symmetric redimerization configuration for the second-layer Si atoms and are energetically favorable.[25] This

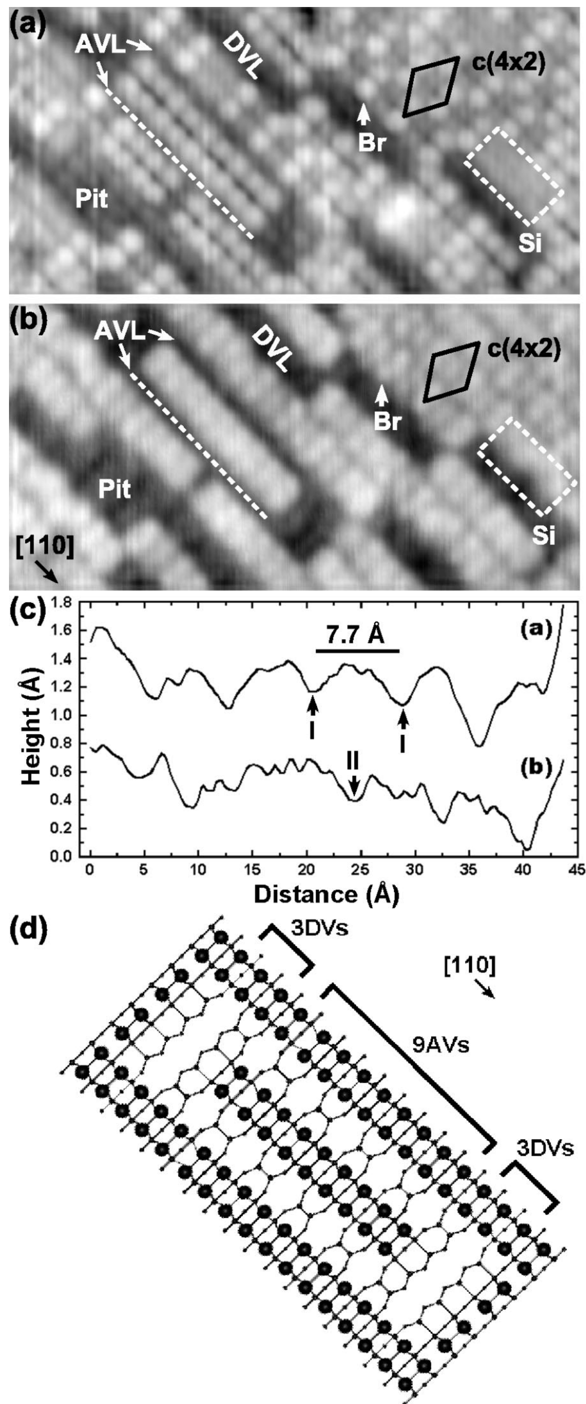

FIG. 5. Empty-state (a) and filled-state (b) images (100×50 Å^2) of a Si(100) that had been exposed to Br and heated to 750 K for 10 min. Images acquired at room temperature reveal bright Br adatoms [best seen in empty-state images (a)]. The Br-$c(4\times2)$ chemisorption structure is indicated, as well as DVL's and AVL's. Height profiles taken along the dashed line show that the exposed second layer Si atoms dimerized (c). The bias dependence of the maxima between empty- and filled-state images is also reflected in the profiles. (d) is a schematic of lines of nine AV's that are terminated with three DV's at each end. Second-layer Si atoms are dimerized but they are depicted as bare for clarity.

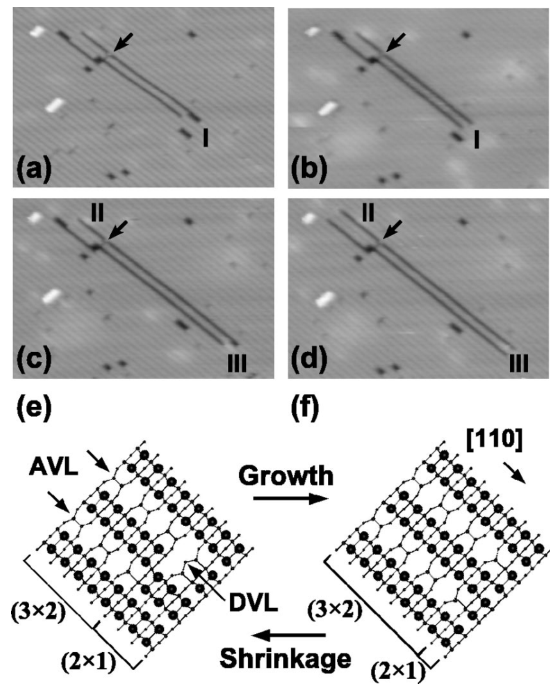

FIG. 6. Images taken at 700 K for a surface with near-saturation Br coverage (250×180 Å^2). Images (a)–(c) were separated by 8 min, while the time between (c) and (d) was 3 min. The AVL's grew with an average rate of 3 Å /min. When AVL's are separated by one dimer row, they have local (3×2) symmetry. The arrow marks the transition between (3×2) and (5×2) regions. Labels I, II, and III indicate AVL growth events, as discussed in the text. Schematics (e) and (f) illustrate growth event III between (c) and (d).

is also the case for atom vacancy lines since second-layer Si atoms symmetrically dimerize with the end Si atoms rebonded, Fig. 5(d). (Although the second-layer dimers can be Br terminated, they are shown bare for clarity.) We conclude that the exposed second-layer Si atoms have formed dimers to produce a local periodicity of (3×2) character.

C. Atom vacancy line growth dynamics

The previous sections have described results obtained with samples that were heated and then imaged at room temperature. To learn about the growth dynamics of atom vacancy lines, we imaged samples that were saturated with Br at room temperature and were then heated on the STM stage. With a variable-temperature STM, we are able to observe the surface evolution after a ~1 h stabilization period. Thereafter, different portions of the surface could be explored or the same area could be scanned for extended periods of time.

Significant atom vacancy line growth, observed in consecutive images, occurred at 700 K. Over time, extremely long pairs of atom vacancy lines formed, with some exceeding 1200 Å in length. Since the width of the atom vacancy lines is 3.8 Å , their aspect ratios can exceed 300, on the order of rare-earth and Bi nanowires grown on Si(100).[6–9]

The images in Fig. 6, obtained at 700 K, show the atom vacancy line growth process on a surface where the initial Br concentration was 0.98 ML. Between Figs. 6(a) and 6(d), the atom vacancy line pair grew from 154 Å (40 dimer units) to

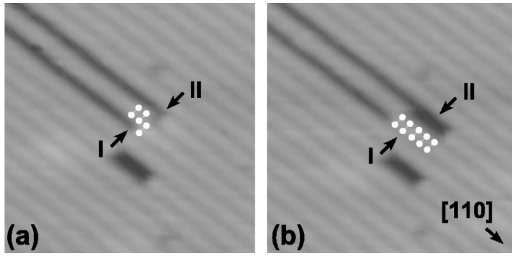

FIG. 7. Images taken 3 min apart at 700 K show the fluctuation in AVL length (80×80 Å ^{2}). Arrow I in (a) marks the end of the AVL, with the upper AVL terminated by a DV, indicated by arrow II. In (b), two new DV's have formed on both sides of the original DV, forming a DVL five dimers long. Two of the DV's were formed when two dimers shifted from the AVL structure toward the lower left.

253 Å (66 units) at an average rate of 3 Å /min. Each of the two atom vacancy lines in Fig. 6(a) is terminated at one end by dimer vacancy lines that are five dimer units in size. The arrow points to a transition point where three dimer vacancies divide the atom vacancy line pair into a local (3×2) segment and a previously unobserved (5×2) segment for Br. During growth, it is common that the (3×2) region consists of a dimer-vacancy-terminated atom vacancy line and a trailing atom vacancy line that is offset by a half-dimer or by a dimer-and-a-half. The trailing atom vacancy line in event I of Fig. 6, for example, advanced when a section of dimers exchanged position with a section of dimer vacancies, splitting the latter and forming two atom vacancy lines. Similar events occurred at II and III since both (3×2) and (5×2) regions advanced between Figs. 6(c) and 6(d).

Figures 6(e) and 6(f) illustrate the lengthening of atom vacancy lines from events I, II, and III. In Fig. 6(e), there are two atom vacancy lines, and the upper atom vacancy line is terminated by two dimer vacancies. As is evident, there are distinct regions with local (3×2) and (2×1) registry. In Fig. 6(f), the displacement of two dimers originally at the end of the lower atom vacancy line allows them to advance by two dimer units. At the same time, the (3×2) region increased and the (2×1) region shrank. Second-layer dimers in the atom vacancy line are shown without Br adatoms. Although we expect Br to terminate some of the dimers in the atom vacancy line, the dynamics at the end of the atom vacancy line require the second layer to be locally Br free. In fact, resaturating a lightly etched surface with Br completely suppressed dimer row shifting at 700 K. This indicates that Br in the atom vacancy line prohibits the dimer shifting observed here.

Further insight into surface dynamics can be gained from the images in Fig. 7 where the atom vacancy line length fluctuates. Arrow I in (a) marks the end of an atom vacancy line, and arrow II marks a single dimer vacancy that terminates the upper line, with the last three dimers indicated. The lower dimer is in (2×1) registry and stays at the site adjacent to the dimer vacancy across the dimer row. The upper two dimers are in (3×2) registry and stay between the two atom vacancy lines. In (b), the atom vacancy line has shrunk by 2 units as the upper two central dimers shifted by one atomic row from the (3×2) to the (2×1) structure. This can be visualized as conversion from Fig. 6(f) to Fig. 6(e). Since the dimer vacancy grew in both directions, two additional dimer vacancies were created between Figs. 7(a) and 7(b). Five dimers are indicated that terminate the two atom vacancy lines. The fact that dimers shift in units of two is consistent with step rearrangement on clean Si(100)-(2×1) because pairwise movement allows second layer Si atoms to dimerize.[33]

D. Roughening and surface evolution at 700 K

In this section, we discuss the evolution of a surface that had an initial Br coverage of 0.98 ML. At 700 K, bare sites were created by gradual Br loss to the gas phase and, together with the initial bare sites, they provided access to the roughening pathway of Fig. 1(b). After 72 h at 700 K, the sample was cooled and the Br concentration was measured to be 0.68 ML. (Quantification of the coverage cannot be done at elevated temperature because of the high mobility of the surface species.) Thus, these results reveal how the morphology and rate of change depends on Br coverage, as discussed in the following paragraphs. Figures 8(a) and 8(b) emphasize the onset of roughening where the appearance of atom vacancy lines, dimer vacancy lines, and regrowth chains could be followed. Figures 9(a) and 9(b) represent the stage where the roughened surface was rich in defects and changes in atom vacancy lines, dimer vacancy lines, and regrowth chains were evident from one image to the next. Figure 10 is representative of a surface dominated by (3×2) areas in both the terrace and the regrowth islands. At this stage, the surface was very dynamic. After ~48 h, the Br concentration had diminished to the point that (3×2) regions began to degrade, and there was recovery of (2×1) regions. Figure 11 shows that the state achieved after 65.7 h had extensive terrace and pit coalescence. This surface was also rapidly changing.

1. Onset and early stages of roughening (~2–8 h at 700 K): Atom vacancy lines, dimer vacancy lines, and regrowth chains

Figures 8(a) and 8(b) focus on an area near an S_B-type step. Dimer rows run diagonally across the image. Over the first few hours, the surface roughened slightly. Small dimer vacancies, dimer vacancy lines, atom vacancy lines, and regrowth chains were distributed sparsely. From Figs. 8(a) and 8(b), there were negligible changes in the step edge. However, the atom vacancy line pair in the upper left lengthened by ~58 dimer units, as highlighted by the dashed lines. New regrowth chains were created, marked with circles, to accommodate Si released during terrace roughening, and some of existing features grew, marked with arrows in Fig. 8(b). Significantly, analysis shows close correlation between regrowth and vacancy areas, indicating roughening without desorption [Fig. 1(b)].

Figures 9(a) and 9(b) are higher-resolution images after 8 h showing that the density of atom vacancy lines, dimer vacancy lines, and bright regrowth chains is much greater. A large fraction of the features changed between Figs. 9(a) and 9(b) as mobile dimer vacancies and Si adatoms created by roughening attached to, or detached from, existing features.

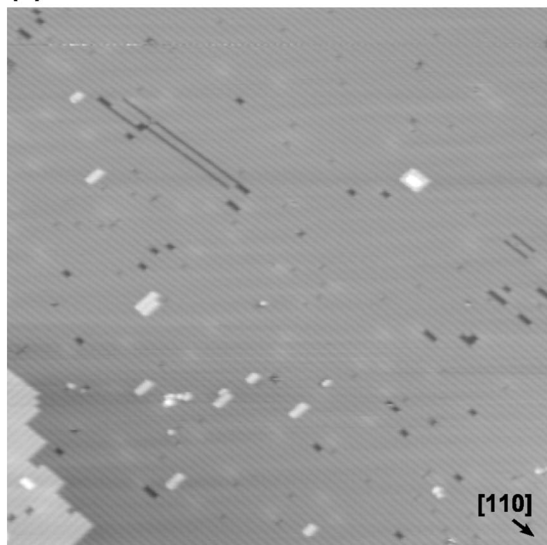

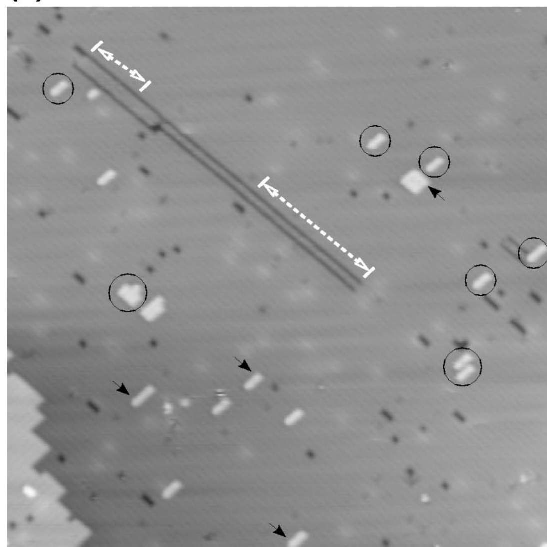

FIG. 8. Images (565×565 Å^2) taken at 700 K showing that the AVL's increased in length by ~58 dimer units. During the same period, the total number of DV's increased by ~14 dimer units and the total number of Si ad-dimers in regrowth structures increased by ~64 dimer units. The difference can be rationalized in terms of isolated Si atoms that cannot be imaged. (Si dimer attachment and detachment at the step edge was negligible.) Hence, surface modification occurs without Si loss (roughening not etching).

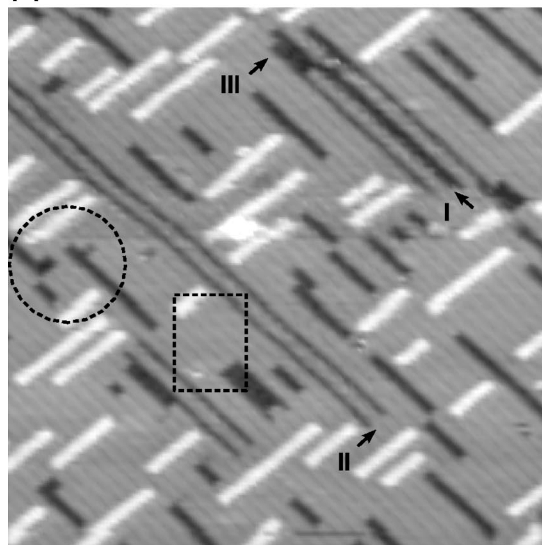

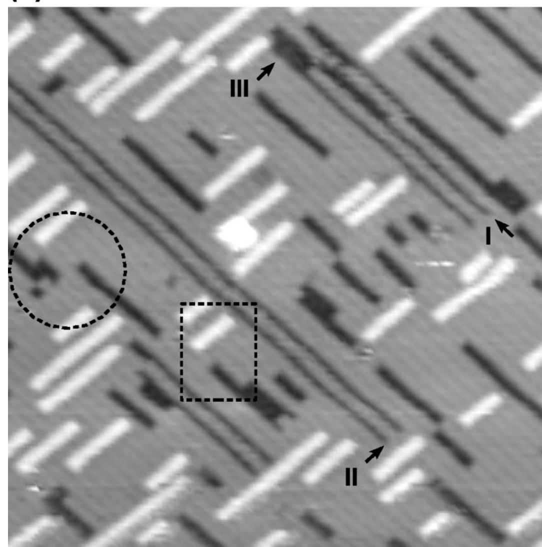

FIG. 9. Consecutive images (320×320 Å^2) after 8 h at 700 K showing long AVL's, small pits, DVL's, and RC's. At this stage, the surface dynamics are greater, as can be seen by comparing the two images. The square marks a region where an equal number of DV's and RC dimers where created. The circle marks a region where several DV's and RC's rearranged. Arrow I points to where part of a dimer row shifted by a single atomic unit. Arrow II points to where the AVL's in (a) grew into a RC. Arrow III indicates where AVL's are terminated by a small pit.

In the circled region, for example, the regrowth chain shifted by one dimer unit toward the lower left and the dimer vacancy lines at the left shrank as two dimer vacancies escaped and the dimer vacancy line at the right captured Si atoms from nearby regrowth chains. Arrow I points to a dimer row where half of the row shifted by one atom unit between Figs. 9(a) and 9(b). We estimate the Br concentration to be 0.93 ML.[34–37] Its reduction is correlated to enhanced roughening and increased surface diffusion.

The evolution from a Br-terminated (2×1) surface to a roughened surface with substantial (3×2) symmetry can be understood from an energetic point of view because the latter is favored. For this surface, Br-Br repulsive interactions destabilize (2×1) areas. Once formed, the atom vacancy lines allow Br atoms on terrace dimers to relax away from each other. Recent calculations by de Wijs and Selloni[15] found that the (3×2) reconstruction for a saturated surface was favored by 15 meV/(1×1). Although favored, the transfor-

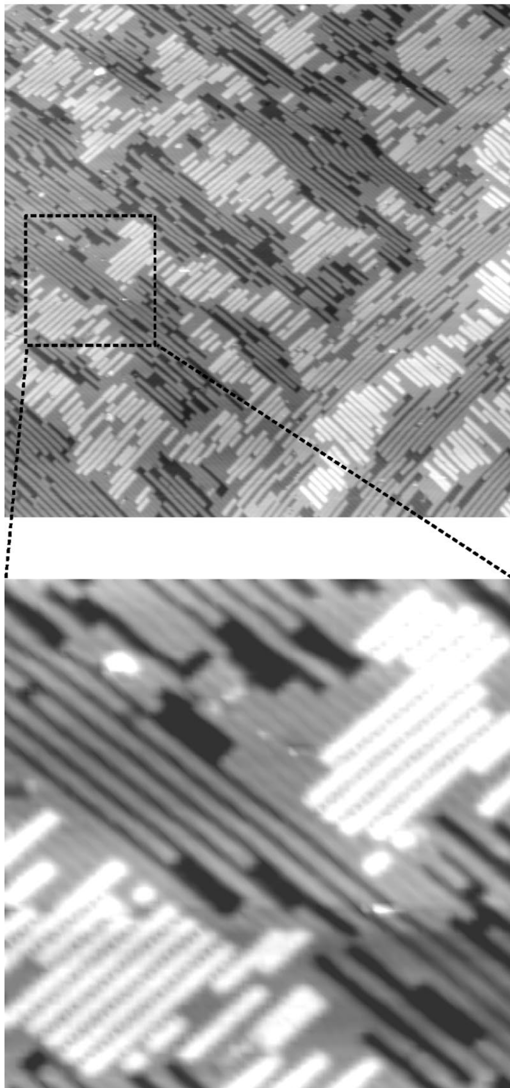

FIG. 10. Large-area image ($\sim 1000\times 1000$ Å^2) taken after 24 h at 700 K shows terraces and RI's with extensive (3×2) reconstruction but also DV structures. The long AVL's restrict the widths of the regrowth islands. Bordering the RI's are regions where the surface has retained the (2×1) reconstruction. The zoomed area reveals the complexity of RC's with (3×2) registry intermixed with those with (2×1) registry and AVL's intermixed with DVL's.

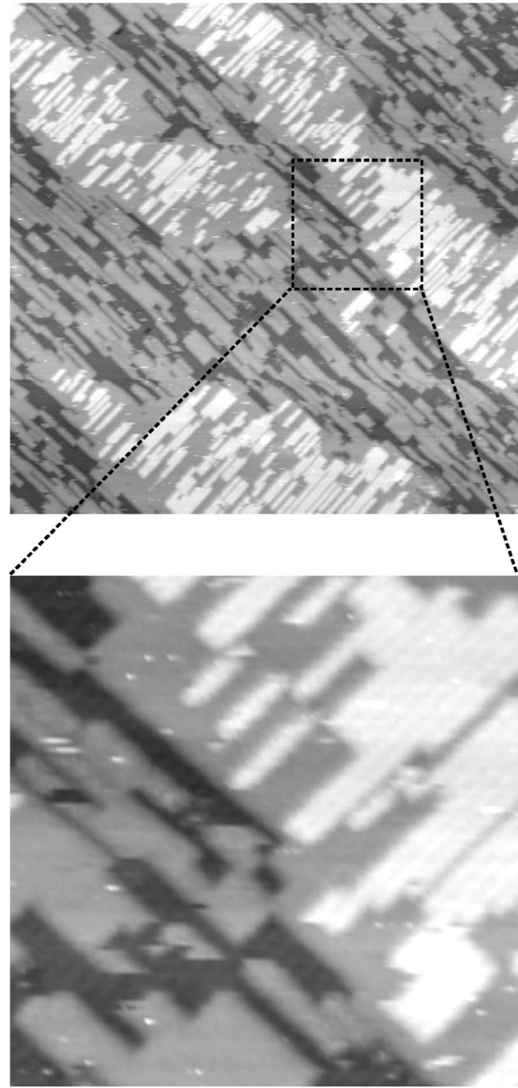

FIG. 11. Large-area image ($\sim 1000\times 1000$ Å^2) taken after 65.7 h at 700 K showing coalescence of terrace vacancies and regrowth features. Both have transformed back to the (2×1) reconstruction, reflecting the loss of Br. The zoomed area shows the dominance of (2×1) registry compared to that in Fig. 10. Six hours after this image was acquired, the sample was cooled to room temperature and the Br concentration was found to be 0.68 ML.

mation is kinetically limited, and bare sites are needed for roughening, Fig. 1(b). In Figs. 9(a) and 9(b), the (3×2) regions are limited to the original terrace.

In many cases, atom vacancy lines at this stage are limited in length because they encounter regrowth chains or two-dimer-wide dimer vacancy lines. The latter stabilize the atom vacancy lines by providing a region that distributes the stress associated with the (3×2) to (2×1) phase shift. Arrow II points to an atom vacancy line pair in Fig. 9(a) that encountered a regrowth chain in Fig. 9(b), while arrow III identifies an atom vacancy line pair that is terminated by a pit. For geometric reasons, regrowth chains are unable to form on (3×2) regions. Their movement is limited to (2×1) regions of the terrace.

2. Maximum patterning (~24–48 h at 700 K): (3×2) terraces and regrowth islands

As surface modification proceeds, the interplay between atom vacancy lines and regrowth islands divides the surface into two main regions: Large areas of (3×2) terraces and areas of (3×2) regrowth islands. [Regrowth chain denotes a chain of regrowth dimers; when they coalesce, we refer to them as islands. Islands have (3×2) symmetry if the chains are separated by an atom row.] This surface represents one that is approaching equilibrium where the (3×2) structure is

energetically favored at high Br concentration and there has been sufficient time at temperature to allow massive atom rearrangement. This divided surface is evident in Fig. 10 where we estimate the Br concentration to be 0.85 ML.[34] The (3×2) reconstructed terrace consists mostly of long atom vacancy line and dimer vacancy line structures, but regrowth islands also show a (3×2) reconstruction with atom vacancy lines separating most of the regrowth islands. If we focus on the zoomed area, we find regrowth chains showing (3×2) registry intermixed with those with (2×1) registry and atom vacancy lines intermixed with dimer vacancy lines. Although the (3×2) configuration is favored, there is local dynamic exchange between these two configurations.

Inspection of Fig. 10 shows that the (2×1) reconstruction persists primarily at the borders of the extended regrowth areas. The regrowth islands are elongated along the dimer row direction. Each regrowth chain in the island is relatively short since growth by Si capture is limited by atom vacancy lines and dimer vacancy lines in the terrace. The Si adatoms can only diffuse, and hence be captured, on (2×1) regions bounded by atom vacancy lines, dimer vacancy lines, and other regrowth features. The atom vacancy lines act as barriers that limit the length of the regrowth chains. Thus, the morphology of Fig. 10 reflects the presence of long atom vacancy lines produced during the initial surface modification, Fig. 8.

Explicit in the discussion of surface evolution is that bare dimers are available so that the roughening pathway of Fig. 1(b) is accessible and atom or vacancy rearrangement is possible. To verify this, we exposed a surface similar to Fig. 10 to resaturate it with Br at room temperature. The sample was then heated to 700 K and imaged. The surface structures were completely frozen, confirming that their mobility requires a certain concentration of bare dimer sites.

3. Recovery stage (>48 h at 700 K)

This section focuses on the stability of the (3×2) areas and its dependence on Br coverage. Previous coverage dependent STM studies by Nakayama *et al*. showed that the (2×1) phase was dominant until ~0.8 ML at 800 K and that the (3×2) phase appeared at high coverage.[18] de Wijs and Selloni[15] subsequently calculated that the (3×2) reconstruction was energetically more stable than the (2×1) when the Br coverage was 1 ML. They also found that the (3×2) reconstruction was unstable for coverages below 2/3 ML. Here, we have the opportunity to examine this stability because we can follow surface changes as the Br concentration diminishes gradually with time.

Figure 10 shows that the (3×2) phase was dominant after 24 h. Figure 11, however, shows a conversion to greater amounts of (2×1) after 65.7 h at 700 K. While elongated regrowth islands are still present, the zoomed image shows that most of the (3×2) areas had converted to (2×1) areas in both the terrace and the islands. This conversion began after ~48 h. After ~72 h, the sample was cooled to room temperature and the final Br coverage was determined to be 0.68 ML. Accordingly, we conclude that the recovery of the (2×1) surface morphology indicates a drop in the concentration below the critical value needed to maintain the (3×2) reconstruction. Though the tendency to convert to the lower energy (2×1) structure is consistent with the calculations by de Wijs and Selloni,[15] the system is dynamic and the rate of change of individual features is high. Even at this coverage, the islands and terraces have mixed character.

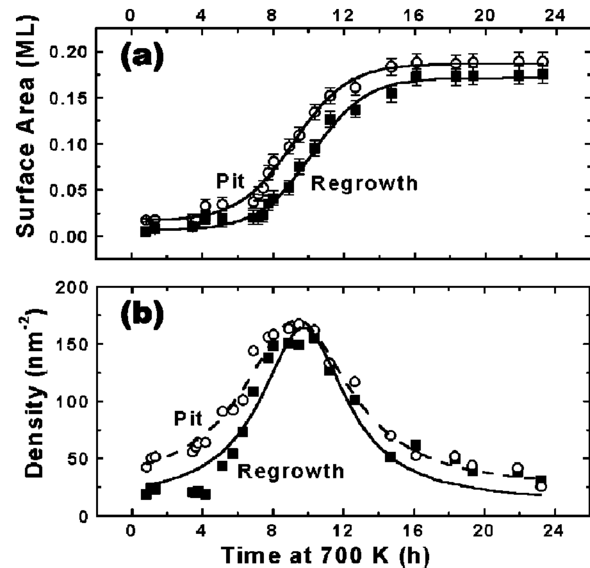

FIG. 12. (a) A plot of pit (DV's plus AVL's) and regrowth areas as a function of time for 24 h after reaching 700 K. The areas increase steadily for the first 10 h, after an initial incubation period, but then begin to level off. After 12 h, the pit and regrowth areas are nearly constant. (b) A plot of the density of pit and regrowth structures showing that both peak after ~9 h and then decreases steadily. The increase in density reflects pit and regrowth creation and the decrease reflects coalescence.

IV. DISCUSSION

The images in Fig. 6 demonstrate that atom vacancy line pairs grow when dimer vacancies split,[25,28,38] but they do not show how the dimer vacancies themselves form. While the model of Nakayama *et al*.[18] described atom vacancy line formation at 800 K in terms of pairwise desorption of $SiBr_2$, it was surprising that it would occur at ~700 K, i.e., the regime here.

Figures 8(a) and 8(b) let us focus on changes for individual features on the surface. Dimers can be resolved and it is possible to count the number of dimer vacancies created and quantify the amount of Si lost during atom vacancy line formation for comparison to the increase of Si ad-dimers in the form of regrowth chains. From Figs. 8(a) and 8(b), the atom vacancy lines increased by ~58 dimer units, the total number of dimer vacancies increased by ~14 dimer units, and total number of Si ad-dimers in regrowth islands increased by ~64 dimer units. The loss of Si dimers from the terrace, 58+14, is close to the increase of Si ad-dimers in regrowth chains, 64, and the difference can be expected to be in the form of individual Si atoms that cannot be imaged at 700 K, as for Si adatoms on clean Si(100). Some might also be lost as additions to the step, though there were negligible changes in the step area imaged. We conclude that atom va-

cancy lines are not formed via pairwise $SiBr_2$ desorption or other pathways that involve Si desorption.

Support for this conclusion comes from analysis of the areas of pits and regrowth as a function of time, as summarized in Fig. 12(a). The increase of pit and regrowth areas is slow at the beginning since the Br coverage is very high. As the Br coverage decreases, the rate of change of the surface increases. From Fig. 12(a), the respective areas have leveled off after $\sim$12 h. Significantly, changes of pit and regrowth areas follow the same trend, and the difference between them is almost constant. This also implies that there is no Si loss.

Yet more evidence about surface processes comes from an experiment in which a saturated surface was prepared at room temperature and was then heated to 700 K for 3 h while exposing it to a constant flux of Br_2. The latter assures saturation but it also makes it possible to determine whether Br_2 impingement at high temperature would activate a new reaction pathway. If the pairwise desorption model were right, more atom vacancy lines would be expected since the Br flux would help to increase the lifetime of intermediate state [$SiBr_2$ Si=Si $SiBr_2$]. In particular, if the central Si dimer were terminated with Br atoms, then the probability of $SiBr_2$ desorption would increase. In fact, imaging of the surface after it was quenched to ambient temperature showed no atom vacancy lines and no other changes to the surface. Accordingly, there is no apparent role of impinging Br_2 on surface modification at 700 K.

The experimental results demonstrate that atom vacancy lines are created by the splitting of preformed dimer vacancy lines as adjacent dimer rows shift by one atomic unit. Indeed, the dynamic conversion between dimer vacancy lines and atom vacancy lines was frequently observed at 700 K. In all cases, these rearrangements required Br free dimers in the atom vacancy lines, as described above. Based on the observed motions of the dimer rows, we speculate that the following processes could be involved as the creation of atom vacancy lines.

Dimer transfer via coupled Si and $SiBr_2$ motion. This process could start by transfer of either a Si atom or a $SiBr_2$ unit produced by the isomerization reaction on a dimer adjacent to the dimer vacancy. After one of these species moves into the dimer vacancy, it would await the arrival of its partner and decay to 2SiBr. de Wijs *et al.*[16] recently calculated the formation energy and barrier of a $SiCl_2$ species on a dimer adjacent to a dimer vacancy on the pristine terrace. They found that, when the dimer was located in the same row with the dimer vacancy, the formation and barrier energies were lowered by 0.3 and $\sim$0.2 eV, respectively, with regard to those of the defect-free sites (lowered from 1.4 and 2.1 eV, respectively). When the dimer is located across the dimer row, the formation energy of a [Si $SiCl_2$] species is lowered by 0.1 eV. Thus, the presence of the defect biases the system to produce Si and $SiBr_2$ units adjacent to dimer vacancies and these units may move in a concerted fashion by jumping one atom distance into the dimer vacancy.

Dimer transfer via coupled SiBr motion. Starting from 2SiBr configuration, the dimer σ bond could be broken to produce two Si-Br units with two back bonds and one dangling bond [breaking the dimer σ bond costs 2.2 eV for Si(100)-(2$\times$1) (Ref. 39)]. Thereafter, the Si-Br unit could move one atom distance into dimer vacancy and the second Si-Br unit could join it to reestablish the dimer σ bond. This process would also result in two atom vacancies separated by a dimer, as observed experimentally.

Surface stress and its ability to alter reaction barriers explains why dimer vacancy creation is more profound at the end of atom vacancy lines compared to other sites on the terrace. It also accounts for the directed growth of atom vacancy lines. For clean Si(100)-(2$\times$1), dimer formation results in surface stress and a large stress anisotropy.[40] Stress is tensile along the dimer bond and compressive along the dimer row. Steric and electrostatic repulsive interactions between halogen adatoms will increase the surface stress, and they are greater for Br than for Cl.[15,21] Additional stress will come from the phase shift between the terrace dimer rows and the central dimer row of the atom vacancy line structure, i.e., the interface between (3$\times$2) and (2$\times$1) in Figs. 6(e) and 6(f).

Figure 12(b) plots the number density of vacancy and regrowth structures over the same period where we counted the number of pits and regrowth regions in either (2$\times$1) or (3$\times$2) structures. An isolated region in the (3$\times$2) structure or a single large structure (pit or regrowth island) is counted as one structure rather than individual atom vacancy lines, dimer vacancy lines, or regrowth chains, while dimer vacancy lines and regrowth chains that are separated by at least one dimer line are counted individually. The increase in the densities is slow for the first few hours because the Br coverage is sufficiently high that roughening pathway via the Br recycling reactions is still limited. With time, Br loss in the form of Br atoms gradually reduces the coverage. After about 4 h, the increase in the densities accelerates. At that time, the Br coverage is still high enough to block the diffusion of Si adatoms and dimer vacancies. After $\sim$9 h, the Br concentration has decreased to the point where significant diffusion can occur, and the surface features begin to coalesce. The areas of surface modification remain about constant, Fig. 12(a), while the densities of pit and regrowth structures decrease, and this reduction reflects a transition of the numerous (2$\times$1) regions into large areas of (3$\times$2) regions providing the first experimental evidence that (3$\times$2) is energetically favorable. Note that the conversion from (3$\times$2) to (2$\times$1) with further decreased Br coverage is not reflected in this figure because after 24 h at 700 K, the Br coverage is still much higher than 2/3 ML.

The question now is how a dimer vacancy can form via the roughening pathway if the initial Br coverage is 0.98 ML. As discussed above, the roughening pathway requires Br-free sites. Experimentally, we found that roughening was slow initially, as expected, but it increased with time, suggesting Br loss and the availability of a greater concentration of bare dimers. To explore this unexpected Br loss effect, we conducted preliminary studies of saturated surfaces that were heated to 700 K for fixed amounts of time and then imaged at room temperature to quantify the extent of Br depletion.[36] Those results indicate that there is Br loss into the gas phase through a channel that had not been detected previously. This was confirmed through results for a sample heated to 750 K,

a temperature where the desorption rate was higher but the onset of vacancy-assisted desorption had not been reached. In particular, a sample with an initial coverage of 0.997 ML had a final coverage of 0.944 after 90 min at 750 K, based on analysis of a total area of $5\times10^4 nm^2 (1.7\times10^5$ dimers). Although dimer vacancies, atom vacancy lines, and regrowth chains were also formed in this 750 K experiment, the extent of Si loss was too low to account for the loss of Br as $SiBr_2(g)$. We also note that a thermal desorption study by Jackman *et al.*[37] detected Br^+ peaks at 500 K and 770 K, and they suggested that it was due to Br atom desorption. We are currently carrying out an extensive study of this phenomenon, with emphasis on the yield and the mechanism underlying atomic halogen loss. This is important because it will shed more light on a system that was once thought to be understood but which is showing unexpected twists at each stage as it is probed more deeply.

V. CONCLUSIONS

We have demonstrated that growth of atom vacancy lines proceeds by dynamic, stress-induced rearrangement of Si and Br atoms at the end of the atom vacancy line. Si atoms ejected from the terrace during this process form regrowth chains. With time at 700 K, the surface undergoes massive rearrangement with large (3×2) reconstructed areas in both the terrace and the regrowth islands. The rate of change for the surface was controlled by the Br coverage, and it is the Br-Br repulsive interaction that is the primary driving force for restructuring. With further decrease in the Br concentration, the (3×2) reconstruction was lost as the surface transformed back to (2×1). As conversion occurred, large islands persisted on the terraces and the atom vacancy lines created at early times served to define their boundaries. The various stages of surface evolution are summarized in Fig. 13, together with their dominant structures. These results demonstrate that extended high-temperature studies of halogen etching are possible, and they offer significant insight into the dynamic processes controlling surface modification and etching.

The stress-induced transformation to (3×2) is analogous to what is observed during Ge growth on Si(100).[41] For monolayer depositions, the lattice mismatch results in increased surface stress that is partially relieved by periodic vacancies along the dimer row.[42] Here, the (3×2) reconstruction relieves the increased stress from Br-Br repulsive interactions.

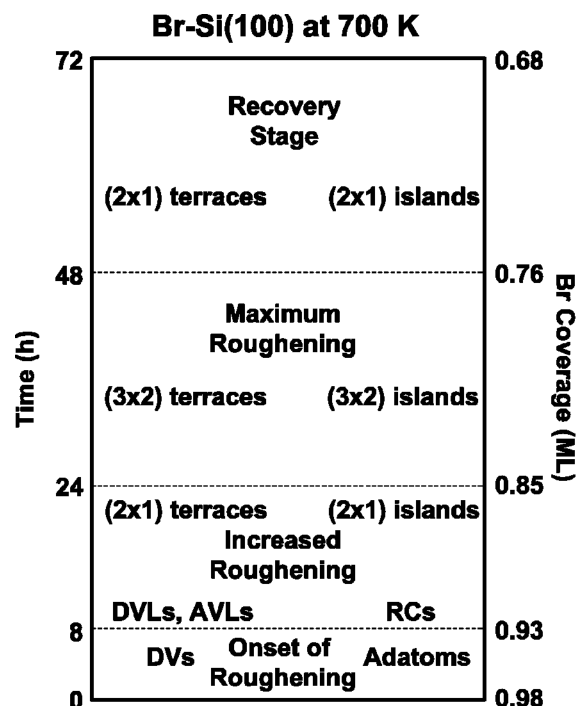

FIG. 13. Summary of the stages of surface roughening and the dominant structures that appeared as a function of heating time. The right axis gives an estimate of the Br concentration.

The directed growth of high aspect ratio structures on Si(100) through a self-regulating process involving localized stress suggests that it may be possible to create longer vacancy structures. It may be possible to use these atom vacancy lines as templates for atomic scale wires through overlayer growth or as atomic scale sensors activated by molecular adsorption in the atom vacancy line.

ACKNOWLEDGMENTS

This study was supported by the National Science Foundation and the U.S. Department of Energy, Division of Materials Sciences under Award No. DEFG02-91ER45439, through the Frederick Seitz Materials Research Laboratory at the University of Illinois at Urbana-Champaign. The experiments were performed in the Center for Microanalysis of Materials, and we gratefully acknowledge the expert assistance of V. Petrova, S. Burdin, and E. Sammann. We thank C. M. Aldao and A. Agrawal for discussions.

*Present address: School of Materials Science & Engineering, Georgia Institute of Technology, Atlanta, GA 30332-0245.

[1] For reviews, see G. E. Poirier, Chem. Rev. (Washington, D.C.) **97**, 1117 (1997); and D. K. Schwartz, Annu. Rev. Phys. Chem. **52**, 107 (2001).

[2] H. H. Song, K. M. Jones, and A. A. Baski, J. Vac. Sci. Technol. A **17**, 1696 (1999).

[3] K. N. Altmann, J. N. Crain, A. Kirakosian, J.-L. Lin, D. Y. Petrovykh, F. J. Himpsel, and R. Losio, Phys. Rev. B **64**, 035406 (2001).

[4] J. M. Moison, F. Houzay, F. Barthe, L. Leprince, E. André, and O. Vatel, Appl. Phys. Lett. **64**, 196 (1994).

[5] J. Tersoff, C. Teichert, and M. G. Lagally, Phys. Rev. Lett. **76**, 1675 (1996).

[6] Y. Chen, D. A. A. Ohlberg, G. Medeiros-Ribeiro, Y. A. Chang, and R. S. Williams, Appl. Phys. Lett. **76**, 4004 (2000).

[7] J. Nogami, B. Z. Liu, M. V. Katkov, C. Ohbuchi, and N. O. Birge, Phys. Rev. B **63**, 233305 (2001).

[8] K. Miki, D. R. Bowler, J. H. G. Owen, G. A. D. Briggs, and K. Sakamoto, Phys. Rev. B **59**, 14868 (1999).

[9] J. H. G. Owen, K. Miki, H. Koh, H. W. Yeom, and D. R. Bowler, Phys. Rev. Lett. **88**, 226104 (2002).
[10] *Morphological Organization in Epitaxial Growth and Removal*, Vol. 14 of *Directions in Condensed Matter Physics*, edited by Z. Zhang and M. G. Lagally (World Scientific, Singapore, 1998).
[11] M. Chander, Y. Z. Li, D. Rioux, and J. H. Weaver, Phys. Rev. Lett. **71**, 4154 (1993).
[12] D. Rioux, R. J. Pechman, M. Chander, and J. H. Weaver, Phys. Rev. B **50**, 4430 (1994).
[13] J. H. Weaver and C. M. Aldao, in Ref. 10, pp. 453–484.
[14] K. Nakayama, C. M. Aldao, and J. H. Weaver, Phys. Rev. Lett. **82**, 568 (1999).
[15] G. A. de Wijs and A. Selloni, Phys. Rev. B **64**, 041402(R) (2001).
[16] G. A. de Wijs, A. De Vita, and A. Selloni, Phys. Rev. Lett. **78**, 4877 (1997).
[17] G. A. de Wijs, A. De Vita, and A. Selloni, Phys. Rev. B **57**, 10021 (1998).
[18] K. Nakayama, C. M. Aldao, and J. H. Weaver, Phys. Rev. B **59**, 15893 (1999).
[19] Z. Dohnálek, H. Nishino, N. Kamoshida, and J. T. Yates, Jr., J. Chem. Phys. **110**, 4009 (1999).
[20] K. S. Nakayama, E. Graugnard, and J. H. Weaver, Phys. Rev. Lett. **88**, 125508 (2002).
[21] C. F. Herrmann, D. Chen, and J. J. Boland, Phys. Rev. Lett. **89**, 096102 (2002).
[22] G. J. Xu, K. S. Nakayama, B. R. Trenhaile, C. M. Aldao, and J. H. Weaver, Phys. Rev. B **67**, 125321 (2003).
[23] C. M. Aldao, S. E. Guidoni, G. J. Xu, K. S. Nakayama, and J. H. Weaver (unpublished).
[24] C. F. Herrmann and J. J. Boland, Phys. Rev. Lett. **87**, 115503 (2001).
[25] G. J. Xu, E. Graugnard, V. Petrova, K. S. Nakayama, and J. H. Weaver, Phys. Rev. B **67**, 125320 (2003).
[26] H. Aizawa, S. Tsuneyuki, and T. Ogitsu, Surf. Sci. **438**, 18 (1999).
[27] K. Hata, T. Kimura, S. Ozawa, and H. Shigekawa, J. Vac. Sci. Technol. A **18**, 1993 (2000).
[28] K. S. Nakayama, E. Graugnard, and J. H. Weaver, Phys. Rev. Lett. **89**, 266106 (2002).
[29] Although the imaging bias was the same for Fig. 4(b) and Fig. 5(a), the contrast between individual features is not exactly the same. This is clear from studies at a fixed bias that the contrast between individual features is dependent on the halogen concentration.
[30] X. Qin and M. Lagally, Phys. Rev. B **59**, 7293 (1999).
[31] D. Rioux, F. Stepniak, R. J. Pechman, and J. H. Weaver, Phys. Rev. B **51**, 10981 (1995).
[32] C. F. Herrmann and J. J. Boland, Surf. Sci. **460**, 223 (2000).
[33] N. Kitamura, B. S. Swartzentruber, M. G. Lagally, and M. B. Webb, Phys. Rev. B **48**, 5704(R) (1993).
[34] We assume that the Br loss can be described as $d\theta(\mathrm{Br})/dt = k\theta(\mathrm{Br})$, where k is a constant.
[35] K. Sinniah, M. G. Sherman, L. B. Lewis, W. H. Weinberg, J. T. Yates, Jr., and K. C. Janda, Phys. Rev. Lett. **62**, 567 (1989).
[36] B. R. Trenhaile, G. J. Xu, A. Agrawal, K. S. Nakayama, and J. H. Weaver (unpublished).
[37] R. B. Jackman, R. J. Price, and J. S. Foord, Appl. Surf. Sci. **36**, 296 (1989)
[38] Herrmann and Boland (Ref. 24) proposed that AVL's grew by capture of single Si vacancies. However, Ref. 28 shows that the single dark features ascribed by HB to single Si vacancies are, in fact, Si dimers with single Br adatoms. Therefore, there is no correlation between the growth of AVL and the single dark features.
[39] Z. Zhang and H. Metiu, Phys. Rev. B **48**, 8166 (1993).
[40] O. L. Alerhand, A. N. Berker, J. D. Joannopoulos, D. Vanderbilt, R. J. Hamers, and J. E. Demuth, Phys. Rev. Lett. **64**, 2406 (1990).
[41] For a thorough review, see F. Liu, F. Wu, and M. G. Lagally, Chem. Rev. (Washington, D.C.) **97**, 1045 (1997).
[42] J. Tersoff, Phys. Rev. B **45**, R8833 (1992).